

Stress analysis model for un-bonded umbilical cables

Xiqia Chen, Shixiao Fu*, Leijian Song, Qian Zhong and Xiaoping Huang

*State Key Laboratory of Ocean Engineering, Shanghai Jiao Tong University,
800 Dongchuan Road, Min Hang, Shanghai, China*

(Received April 18, 2013, Revised June 7, 2013, Accepted June 10, 2013)

Abstract. For the optimization design and strength evaluation of the umbilical cable, the calculation of cross section stress is of great importance and very time consuming. To calculate the cross section stress under combined tension and bending loads, a new integrated analytical model of umbilical cable is presented in this paper. Based on the Hook's law, the axial strain of helical components serves as the tensile stress. Considering the effects of friction between helical components, the bending stress is divided into elastic bending stress and friction stress. For the former, the elastic bending stress, the curvature of helical components is deduced; and for the latter, the shear stress before and after the slipping of helical components is determined. This new analytical model is validated by the experimental results of an umbilical cable. Further, this model is applied to estimate the extreme strength and fatigue life of the umbilical cable used in South China Sea.

Keywords: un-bonded umbilical; stress analysis model; axial stiffness; bending stiffness

1. Introduction

Multilayered un-boned umbilical are widely used in offshore production, conveying fluid, signals and power between well-heads and offshore rigs. The main advantage of un-bonded umbilicals is that they are compliant and highly deformable in bending, but also quite stiff in tension, which enables them to undergo large deformations induced by currents, waves, vortex-induced vibrations and the motion of floating vessels. To ensure the safety in their serving life, it is indispensable to conduct the extreme and fatigue analysis for un-bonded umbilicals at design stages. However, due to the complexity of the umbilical's structural section, stress calculation, serving as the core of the analysis, is quite difficult and time-consuming.

Several similar multilayered cable structures such as flexible pipes, marine cables and umbilicals are widely used in ocean engineering, and the prediction of their axial stiffness, bending stiffness and cross section stress distribution become the focus of the design. Based on the strain analysis of multilayered structures under axial loads, Knapp (1979), Costello (1997) and Witz (1996) neglected the radius reduction effects of the helical components when studying the cross section tensional stiffness properties of the ropes and flexible pipes. From their results, axially symmetric relationships between the axial loads and the strains have been found; and the prediction achieved good agreements with experimental results. However, when it comes to the

*Corresponding author, Professor, E-mail: shixiao.fu@sjtu.edu.cn

tensional stiffness of the un-bonded umbilical, the effects of the radius reduction caused the predicted result 2-4 times larger than the experimental result (Ekeberg *et al.* 2006). As for the bending properties of the multi layer structures, more difficulties is confronted with due to the large nonlinearity behaviors caused by the sliding of the helical components. Assuming that helical components can slide along both of the axial and transversal direction, Ferét and Bournazel (1987) presented their stress and displacement analytical model for dynamically bent un-bounded flexible pipes, which has been widely accepted. To further consider the effects of the transversal sliding constrains on the helical components, based on the assumption that the transverse sliding was entirely constrained by the structural restrictions and only sliding along the axis directions was allowed, Witz and Tan (1996) developed a more general analytical model for the prediction of the bending stiffness of the multi-layer cable structures, e.g., flexible pipes, marine cables and umbilicals. To get the stress of the flexible pipes under bending loads, Saevik (2011) proposed analytical models by dividing the bending stress into elastic part and friction part, where the elastic bending stress was derived based on the loxodromic curve assumption and friction stress by the shear stress of helical components. As mentioned above, great efforts have been made to predict the behaviors of multilayered structures under tension and bending loads, but few efforts were shown regarding stress predictions for the un-bonded umbilical, which is in great need and hence important for the extreme and fatigue analysis in the design.

Taking the sliding of individual helical components into consideration, analytical stress and stiffness models for un-bonded umbilical are developed in this paper. Combining the proposed analytical stress model with standard dynamic response simulation method (Martins and Pesce (2002), Knapp (2004), Thies, Johannning and Smith (2011)), simplified methods for the extreme and fatigue strength evaluation of un-bonded umbilical are obtained. Meanwhile, a given numerical case demonstrates the reliability of the stress model in practical designs.

2. Stress in umbilical

2.1 Tensile stress

The geometric configuration of a helical component is shown in Fig. 1, and the lay angle α can be expressed as

$$\tan \alpha = \frac{\phi R}{l} \quad (1)$$

where R denotes the lay radius of the helical component, ϕ denotes the rotation angle of the helical component around the centerline of the umbilical and l denotes the length of the umbilical segment

According to the geometric relationship between the original and deformed shapes, after an axial elongation Δu as illustrated in Fig.1, the axial strain in the elongated helical component can be written as

$$\varepsilon = \frac{a' - a}{a} \quad (2)$$

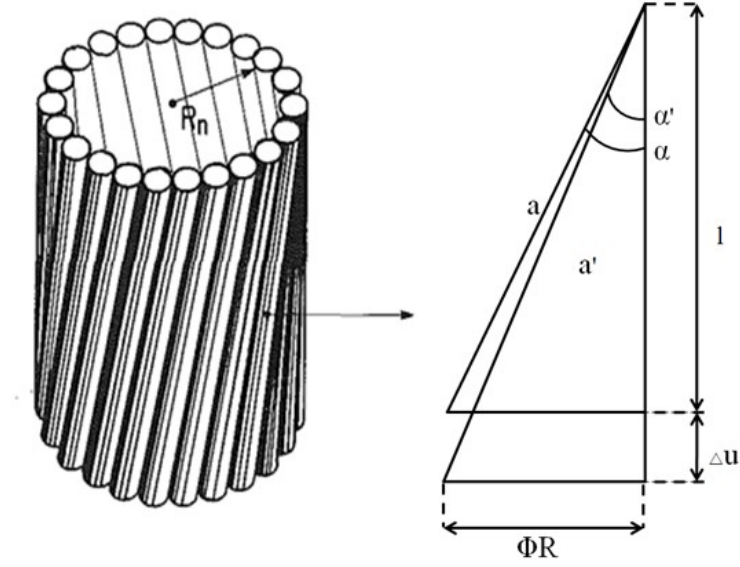


Fig. 1 Helical geometry of a helical component

where a and a' are the length of the helical component before and after the elongation respectively, and can be expressed as

$$a = \frac{l}{\cos \alpha} \quad (3)$$

$$a' = \frac{l + \Delta u}{\cos \alpha'} \quad (4)$$

According to Fig.1, the lay angle after the elongation can be expressed as

$$\cos \alpha' = \frac{l + \Delta u}{\sqrt{(l + \Delta u)^2 + (l \tan \alpha)^2}} \quad (5)$$

Substituting Eqs. (3)-(5) into Eq. (2), we have

$$\varepsilon = \sqrt{(1 + \Delta u / l)^2 \cos^2 \alpha + \sin^2 \alpha} - 1 \quad (6)$$

Neglecting the second-order strain quantities, Eq. (6) can be linearized as

$$\varepsilon = \frac{\Delta u \cos^2 \alpha}{l} \quad (7)$$

According to the Hooke's law, we have

$$\sigma_a = \frac{\Delta u E \cos^2 \alpha}{l} \quad (8)$$

$$F_a = \frac{\Delta u EA \cos^2 \alpha}{l} \quad (9)$$

where σ_a , F_a and E denote the axial stress, axial force and the material elastic modulus of the helical component respectively.

Projecting the axial force of the helical component onto the axes of the umbilical, the force contribution from the helical component to the total axial force of the umbilical can be further deduced

$$F_a' = \frac{\Delta u EA \cos^3 \alpha}{l} \quad (10)$$

The axial stress σ_a'' and axial force F_a'' of the straight component can be deduced directly based on the Hooke's law as

$$\sigma_a'' = \frac{\Delta u E}{l} \quad (11)$$

$$F_a'' = \frac{\Delta u EA}{l} \quad (12)$$

Based on Eqs. (10) and (12), the total axial force F of the umbilical with axial elongation Δu can be deduced as

$$F = \sum_{i=1}^n \frac{\Delta u A_i E_i \cos^3 \alpha_i}{l} + \sum_{j=1}^m \frac{\Delta u A_j E_j}{l} \quad (13)$$

where $E_i A_i$ denotes the axial stiffness of helical component i ; α_i denotes the lay angle of helical component i ; n denotes the number of helical components; l denotes the length of the umbilical; $E_j A_j$ denotes the axial stiffness of straight component j ; m denotes the number of straight components.

The axial stiffness K_a of the umbilical can further be derived from Eq. (13) as

$$K_a = \frac{F}{\Delta u / l} = \sum_{i=1}^n A_i E_i \cos^3 \alpha_i + \sum_{j=1}^m A_j E_j \quad (14)$$

2.2 Bending stress

The bending stress in helical components section can be divided into elastic bending stress and friction stress, which are respectively caused by the deformation of the materials and the frictional forces between adjacent components. The following assumptions are made for the further derivation of the bending stress.

- (1). Helical components can only slide along their own axes (Seavik (2011)).
- (2). Interlayer contact pressure is constant throughout the interface, and the changes in contact pressure induced by bending itself can be ignored.
- (3). Static and dynamic friction coefficients are equal.
- (4). Only full stick and full slip states are considered (Ferét and Bournazel (1987), Witz and Tan (1996)).

2.2.1 Elastic bending stress

A right-handed Cartesian coordinate is used to describe the geometry of the umbilical helical components, as shown by Fig.2. The origin is fixed at the centroid of the umbilical cross section; the Z-axis is parallel to the initial centerline of the umbilical and the X-axis parallels with the neutral axis of bending.

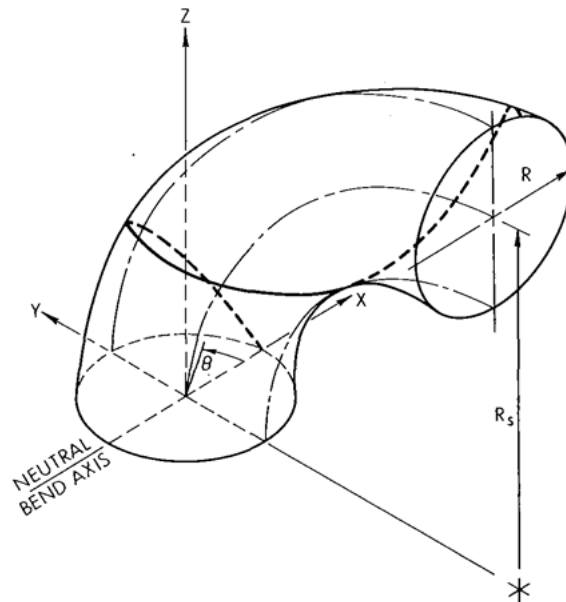


Fig. 2 The Cartesian coordinate of the umbilical

In this coordinate system, the position vector \mathbf{r} of the point on the helical component can be expressed as a function of the polar angel θ

$$\mathbf{r} = \begin{pmatrix} R \cos \theta \\ R_s [1 - \cos k\theta (1 - \delta \sin \theta)] \\ R_s (1 - \delta \sin \theta) \sin k\theta \end{pmatrix} \quad (15)$$

where R_s denotes the bending radius of the umbilical segment, δ and k are defined as

$$\delta = R / R_s \quad (16)$$

$$k = \delta / \tan \alpha \quad (17)$$

The parametric curvature vector $\boldsymbol{\kappa}$ of helical components can be expressed (Lipschutz (1969)) in the Cartesian reference frame as

$$\boldsymbol{\kappa} = \frac{\mathbf{r}' \times \mathbf{r}''}{|\mathbf{r}'|^3} \quad (18)$$

where \mathbf{r}' and \mathbf{r}'' denote the first and second derivatives, respectively, of the position vector of the point on the helical components with respect to polar angel θ .

Substituting Eq. (15) into Eq. (18), we can obtain the curvature vector of the helical component as

$$\boldsymbol{\kappa} = \begin{pmatrix} \frac{Y'Z'' - Z'Y''}{[X'^2 + Y'^2 + Z'^2]^{3/2}} \\ \frac{Z'X'' - X'Z''}{[X'^2 + Y'^2 + Z'^2]^{3/2}} \\ \frac{X'Y'' - Y'X''}{[X'^2 + Y'^2 + Z'^2]^{3/2}} \end{pmatrix} \quad (19)$$

where X' , Y' , Z' , X'' , Y'' and Z'' denote the first and second derivatives of the point coordinates on the helical component with respect to polar angel θ ; which can be expressed as

$$\begin{aligned} X' &= -R \sin \theta \\ Y' &= kR_s \sin k\theta - \delta kR_s \sin k\theta \sin \theta + \delta R_s \cos k\theta \cos \theta \\ Z' &= kR_s \cos k\theta - \delta kR_s \cos k\theta \sin \theta - \delta R_s \sin k\theta \cos \theta \end{aligned} \quad (20)$$

$$\begin{aligned} X'' &= -R \cos \theta \\ Y'' &= k^2 R_s \cos k\theta - \delta(1+k^2)R_s \cos k\theta \sin \theta \\ Z'' &= -k^2 R_s \sin k\theta + \delta(1+k^2)R_s \sin k\theta \sin \theta - 2\delta kR_s \cos k\theta \cos \theta \end{aligned} \quad (21)$$

To illustrate the change of curvature before and after bending, the curvature vector should be

projected to normal and bi-normal directions as shown in Fig. 3.

Normal and bi-normal directions of helical component can be expressed as

$$\kappa_n = \mathbf{\kappa} \cdot \mathbf{n}_n \quad (22)$$

$$\kappa_b = \mathbf{\kappa} \cdot \mathbf{n}_b \quad (23)$$

where κ_n and κ_b denote the curvatures of the helical component in normal and binormal directions respectively; \mathbf{n}_n and \mathbf{n}_b denote the normal and binormal direction vector of the helical component respectively and can be expressed as

$$\mathbf{n}_n = \begin{pmatrix} R \cos \theta \\ R \sin \theta \cos \alpha \\ -R \sin \theta \sin \alpha \end{pmatrix} \quad (24)$$

$$\mathbf{n}_b = \begin{pmatrix} R^2 \cos^2 \alpha - \frac{R^3 \sin \theta \cos \alpha}{R_s} \\ R^2 \cos^2 \alpha - \frac{R^3 \sin \theta \cos^2 \alpha}{R_s} - R^2 \sin \alpha \\ R^2 \cos^2 \alpha - \frac{R^3 \sin \theta \cos^2 \alpha}{R_s} + R^2 \cos \alpha \end{pmatrix} \quad (25)$$

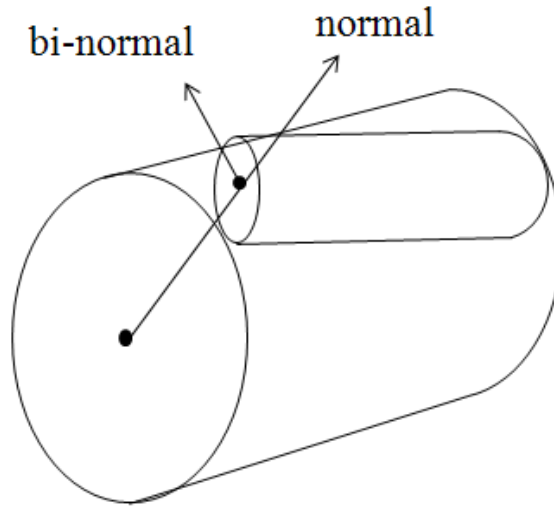


Fig. 3 Normal and bi-normal directions of helical component

Substituting Eqs. (19) and (24) into Eq. (22), and substituting Eqs. (19) and (25) into Eq. (23),

we can obtain the curvature expressions of the helical component in normal and binormal directions

$$\kappa_n = \frac{(1 + \sin^2 \alpha) \cos \alpha \cos \theta}{R_s} \quad (26)$$

$$\kappa_b = \frac{\sin^2 \alpha}{R} - \frac{(\cos^2 \alpha - \sin^2 \alpha) \sin^2 \alpha \sin \theta}{R_s} \quad (27)$$

When the bend radius R_s is infinite, i.e., the umbilical is in straight configuration, the curvatures of the helical component become

$$\kappa_{n0} = 0 \quad (28)$$

$$\kappa_{b0} = \frac{\sin^2 \alpha}{R} \quad (29)$$

Subtracting (28) from (26), and (29) from (27), the corresponding curvature changes in both normal and binomial directions can be expressed as

$$\Delta \kappa_n = \frac{(1 + \sin^2 \alpha) \cos \alpha \cos \theta}{R_s} \quad (30)$$

$$\Delta \kappa_b = -\frac{(\cos^2 \alpha - \sin^2 \alpha) \sin^2 \alpha \sin \theta}{R_s} \quad (31)$$

Since the normal and binormal curvatures are orthogonal with each other, the total bending curvature change of the bending helical component can be expressed as

$$\Delta \kappa = (\Delta \kappa_n^2 + \Delta \kappa_b^2)^{1/2} \quad (32)$$

As a matter of fact, the curvature changes in the binormal direction affect the extreme curvature change little and hence can be neglected (Witz and Tan (1995)). Then the total curvature change can be written as

$$\Delta \kappa = \frac{(1 + \sin^2 \alpha) \cos \alpha \cos \theta}{R_s} \quad (33)$$

According to the bending theory of Euler's beam, the maximum elastic bending strain ε_e , the maximum elastic bending stress σ_e and the corresponding bending moment M_e of the helical component can be written as

$$\varepsilon_e = \frac{r(1 + \sin^2 \alpha) \cos \alpha \cos \theta}{R_s} \quad (34)$$

$$\sigma_e = \frac{Er(1 + \sin^2 \alpha) \cos \alpha \cos \theta}{R_s} \quad (35)$$

$$M_e = \frac{EI(1 + \sin^2 \alpha) \cos \alpha \cos \theta}{R_s} \quad (36)$$

where r and I denote the radius and inertia moment of the cross section of the helical component, respectively.

2.2.2 Friction stress

For modest curvatures, the shear forces of the helical component are smaller than the friction forces between the components and the cylinders. Within this curvature range, the un-bonded umbilicals will deform as an integrated solid structure, where the axial strain ε_f in the helical component section can be defined by

$$\varepsilon_f = \frac{ds}{ds_0} - 1 \quad (37)$$

where ds_0 and ds denote the differential lengths of helical components before and after bending respectively, which can be determined by the following equation

$$ds = [X'^2 + Y'^2 + Z'^2]^{1/2} d\theta \quad (38)$$

Substituting Eqs. (20) and (38) into Eq. (37) and neglecting higher-order terms, we can get ε_f as

$$\varepsilon_f = \frac{R \cos^2 \alpha \sin \theta}{R_s} \quad (39)$$

Based on the Hook's law, the axial stress σ_f and axial force F_f on the helical component due to friction can be expressed as

$$\sigma_f = \frac{ER \cos^2 \alpha \sin \theta}{R_s} \quad (40)$$

$$F_f = \frac{EAR \cos^2 \alpha \sin \theta}{R_s} \quad (41)$$

Differentiating Eq. (41) with respect to the length s' given in $\theta = \frac{\sin \alpha}{R} s'$, the shear force f_f per unit length along the helical component can be obtained as

$$f_f = \frac{EA \cos^2 \alpha \sin \alpha \cos \theta}{R_s} \quad (42)$$

When bending curvature continuously increases to a critical value, the friction between layers is insufficient to restrict the shear force of the helical component, and the slipping will occur along the axes. At this moment, the shear force is equal to friction force, whose expression can be obtained

$$f = \mu(q^i + q^e) \quad (43)$$

where μ denotes the friction coefficient which is assumed to be equal for internal and external surface; q^i and q^e denote the contact pressure on the internal and external surface of the helical component produced by tension forces F and pressure forces P , which can be expressed as

$$q^i = q^e = \frac{FEA \cos^2 \alpha_i \sin^2 \alpha_i}{R_i K_a} + \frac{2\pi R_i P}{k_i} \quad (44)$$

where α_i , R_i and k_i denotes the lay angel, lay radius and number of the helical components in layer i ; K_a denotes the axial stiffness of the umbilical.

Equating f with f_f , the critical bending radius R_{yc} can be obtained as

$$R_{yc} = \frac{EA \cos^2 \alpha \sin \alpha}{\mu(q^i + q^e)} \quad (45)$$

According to assumption (3), the helical component will reach full slip state when the umbilical bends over the critical radius. Under this state, the shear stress along the helical component is the constant. By integrating the shear stress, friction stress σ_f' and friction force F_f' can then be determined

$$\sigma_f' = \int_0^\theta \frac{\mu(q^i + q^e)}{A} d \frac{R\theta}{\sin \alpha} = \frac{\mu R(q^i + q^e)}{A \sin \alpha} \theta \quad (46)$$

$$F_f' = \frac{\mu R(q^i + q^e)}{\sin \alpha} \theta \quad (47)$$

Incorporated Eqs. (40) and (46), the friction stress of the helical component under different curvature can be expressed as

$$\sigma_f = \begin{cases} \frac{ER \cos^2 \alpha \sin \theta}{R_s} & R_s \geq R_{yc} \\ \frac{\mu R \theta (q_r^i + q_r^e)}{A \sin \alpha} & R_s < R_{yc} \end{cases} \quad (48)$$

The bending moment of the helical component due to friction can be further deduced from Eqs. (41) and (47)

$$M_f = \begin{cases} \frac{EAR^2 \cos^3 \alpha \sin^2 \theta}{R_s} & R_s \geq R_{yc} \\ \frac{\mu R^2 (q^i + q^e)}{\tan \alpha} \theta \sin \theta & R_s < R_{yc} \end{cases} \quad (49)$$

Adding up the elastic bending stress and friction stress, we can obtain the maximum bending stress in the cross section of the helical component as

$$\sigma_b = \begin{cases} \frac{Er(1+\sin^2 \alpha) \cos \alpha \cos \theta}{R_s} + \frac{ER \cos^2 \alpha \sin \theta}{R_s} & R_s \geq R_{yc} \\ \frac{Er(1+\sin^2 \alpha) \cos \alpha \cos \theta}{R_s} + \frac{\mu R \theta (q_r^i + q_r^e)}{A \sin \alpha} & R_s < R_{yc} \end{cases} \quad (50)$$

As expressed in Eq. (50), the bending stress is a function of bending curvature, interlayer friction coefficient and interlayer contact pressure.

The stress σ' and moment M' of the straight component in the umbilical can be deduced directly according to the bending theory of Euler's beam as

$$\sigma' = E' r' / R_s \quad (51)$$

$$M' = E' I' / R_s \quad (52)$$

where, r' , E' and I' denote the radius, the elastic modulus and the inertia moment of the straight component respectively.

The total bending moment of the umbilical subjected to bending radius R_s can be obtained by adding moments of helical components and those of straight components, as following

$$M = \begin{cases} \sum_{k=1}^r \sum_{i=1}^n \left(\frac{E_k I_k (1 + \sin^2 \alpha_k) \cos \alpha_k \cos \theta_i}{R_s} + \frac{E_k A_k R_k^2 \cos^3 \alpha_k \sin^2 \theta_i}{R_s} \right) + \sum_{j=1}^m \frac{E_j I_j}{R_s} & R_s \geq R_{yc} \\ \sum_{k=1}^r \sum_{i=1}^n \left(\frac{E_k I_k (1 + \sin^2 \alpha_k) \cos \alpha_k \cos \theta_i}{R_s} + \frac{\mu_k R_k^2 (q^i + q^e)}{\tan \alpha_k} \theta_i \sin \theta_i \right) + \sum_{j=1}^m \frac{E_j I_j}{R_s} & R_s < R_{yc} \end{cases} \quad (53)$$

where $E_k A_k$ and $E_k I_k$ denotes the axial stiffness and bending stiffness, respectively, of helical components in layer k ; α_k and R_k denotes the lay angle and lay radius, respectively, of helical component in layer k ; μ_k denotes the friction coefficient of helical components in layer k ; θ_i denotes the polar angle of helical component i in layer k ; n denotes the number of helical components in layer k ; r denotes the number of the helical layers; $E_j I_j$ denotes the bending stiffness of straight component j ; m denotes the number of straight components.

The bending stiffness K_b can be further deduced as

$$K_b = \begin{cases} \sum_{k=1}^r \sum_{i=1}^n (E_k I_k (1 + \sin^2 \alpha_k) \cos \alpha_k \cos \theta_i + E_k A_k R_k^2 \cos^3 \alpha_k \sin^2 \theta_i) + \sum_{j=1}^m E_j I_j & R_s \geq R_{yc} \\ \sum_{k=1}^r \sum_{i=1}^n E_k I_k (1 + \sin^2 \alpha_k) \cos \alpha_k \cos \theta_i + \sum_{j=1}^m E_j I_j & R_s < R_{yc} \end{cases} \quad (54)$$

2.3 Analytical model for the stress

Combining Eq. (8) with Eq. (50), we can express the stresses of helical components subject to tension F and bending radius R_s as

$$\sigma = \eta F + \lambda / R_s \quad (55)$$

where η and λ can be determined by

$$\eta = E \cos^2 \alpha / K_a \quad (56)$$

$$\lambda = \begin{cases} Er(1 + \sin^2 \alpha) \cos \alpha \cos \theta + ER \cos^2 \alpha \sin \theta & R_s \geq R_{yc} \\ Er(1 + \sin^2 \alpha) \cos \alpha \cos \theta + \frac{\mu R_s \theta (q_r^i + q_r^e)}{A \sin \alpha} & R_s < R_{yc} \end{cases} \quad (57)$$

For the helical tendons, the equivalent stress is in terms of the axial stresses and can be calculated by Eq. (56); as to the helical tubes, the equivalent stress should be the von Mises stress, and can be expressed in cylinder coordinate system as

$$\sigma_e = \sqrt{\frac{(\sigma_h - \sigma_a)^2 + (\sigma_a - \sigma_r)^2 + (\sigma_h - \sigma_r)^2}{2}} \quad (58)$$

where σ_a , σ_h and σ_r denote the axial stress, the hoop stress and the radius stress respectively
Axial stress can be defined as

$$\sigma_a = \sigma_{aTension} + \sigma_{aBending} + \sigma_{aPressure} \quad (59)$$

in which $\sigma_{aTension}$ and $\sigma_{aBending}$ can be calculated by stress analysis model Eq. (56). The axial stress caused by pressure $\sigma_{aPressure}$ can be expressed as

$$\sigma_{aPressure} = \frac{P_i r_i^2 - P_o r_o^2}{r_o^2 - r_i^2} \quad (60)$$

where P_i and P_o denote inner and outer pressure respectively; r_i and r_o denote inner and outer radius of tubes respectively.

Hoop stress can be defined as (ISO 13628-5 (2005))

$$\sigma_h = \frac{r_o + r_i}{2(r_o - r_i)} (P_i - P_o) \quad (61)$$

Radius stress varies with wall thickness $r(x)$ and can be expressed as (DNV-OS-F101 (2005))

$$\sigma_r = \frac{P_i r_i^2 - P_o r_o^2}{r_o^2 - r_i^2} + \frac{r_i^2 (P_o - P_i)}{r(x)^2 (r_o^2 - r_i^2)} \quad (62)$$

2.4 Extreme strength evaluation

Assuming the equivalent stress σ_e equals with $\eta_\sigma \sigma_{SMYS}$, we can get the governing equations of extreme capacity curve for helical tendons and for helical tubes respectively as

$$\eta F + \lambda / R_s = \eta_\sigma \sigma_{SMYS} \quad (63)$$

$$\eta F + \lambda / R_s = [(\sigma_h + \sigma_r) + (\sigma_h + \sigma_r)^2 - 4(\sigma_r^2 + \sigma_h^2 - \sigma_h \sigma_r - \eta_\sigma^2 \sigma_{SMYS}^2)]^{1/2} / 2 - \sigma_{aPressure} \quad (64)$$

where σ_{SMYS} and η_σ denote the material ultimate strength and the utilization factor respectively.

According to Eqs. (63) and (64), the extreme strength of the umbilical will depend on the equivalent stress level from both of the tension forces and bending moment. Therefore, the stress deduced by both tension and bending loads should be less than the extreme stress of the materials in the umbilical.

2.5 Extreme strength and fatigue life evaluation procedures

By combining the stress analysis model with standard dynamic numerical simulation procedures for the risers, we can evaluate the extreme capacity and fatigue life of the un-bonded umbilical. The evaluation procedures can be expressed in the following chart

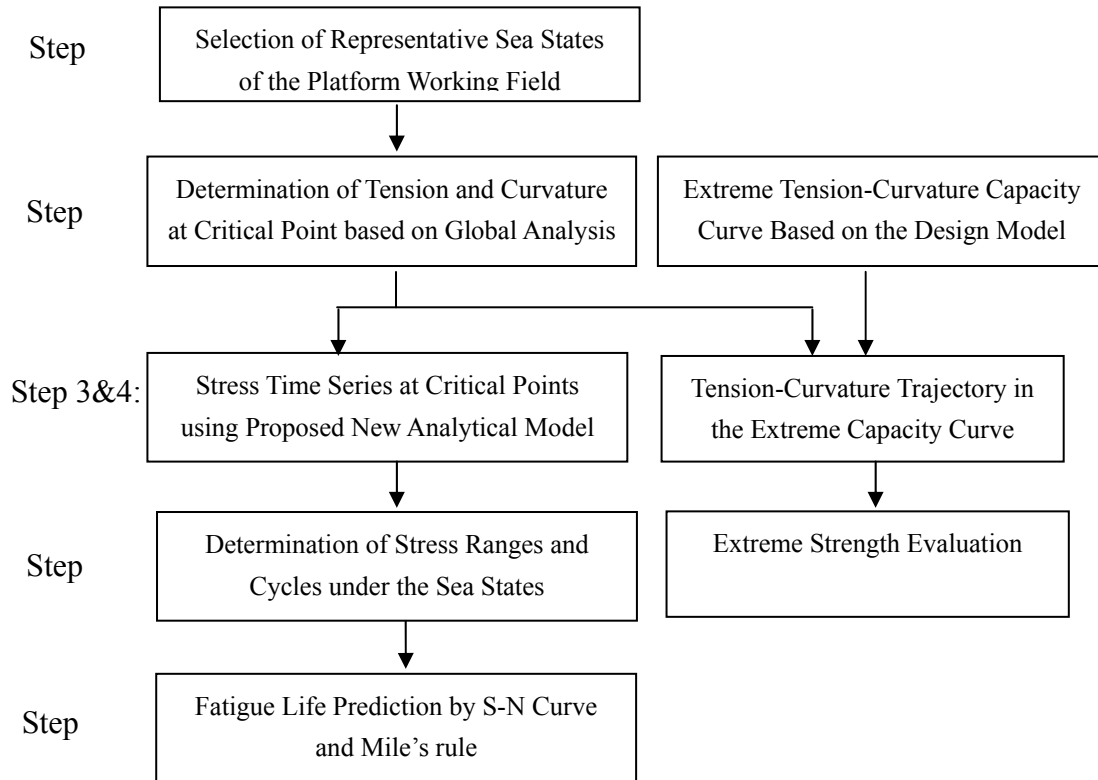


Fig. 4 Un-Bonded umbilical extreme strength and fatigue life estimation procedures

3. Numerical example

3.1 Basic data of the example umbilical

A representative umbilical, as shown in Fig. 5, is set to apply the proposed analytical stress model in extreme strength and fatigue life evaluations. Its global geometrical parameters, cross section and material properties are listed in Table 1 and Table 2.

3.2 Axial and bending stiffness

The axial and bending stiffness of the example umbilical, calculated by Eqs. (14) and (53) and measured from corresponding experiments, are plotted in Figs. 6 and 7, in which the slopes of the curves indicate the axial and bending stiffness.

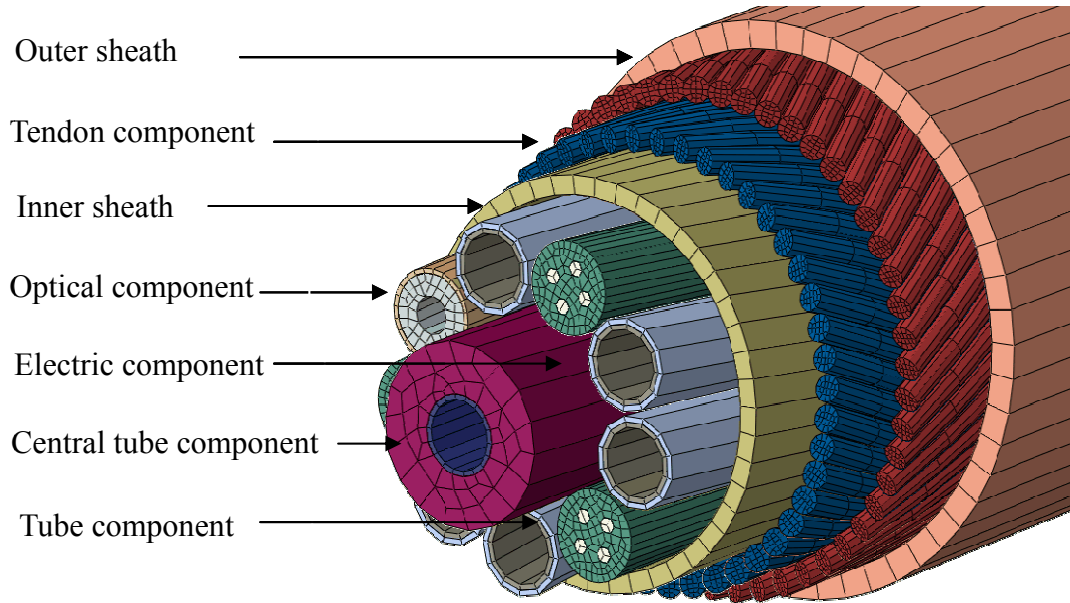


Fig.5 Un-Bonded umbilical extreme strength and fatigue life estimation procedures

Table 1 Global Configuration Parameters of the Umbilical

Total length	2000	[m]
Top angle	84	°
Suspended length	1519.5	[m]
Touchdown position	652.7	[m]
Laying Length	480.5	[m]

Table 2 Cross section and material properties of the umbilical

Tube	Diameter	12.7	[mm]
	Thickness	1	[mm]
	Yield Stress	630	[MPa]
	Elastic Modulus	210	[GPa]
	Inner pressure	34.5	[MPa]
Tendon	Diameter	5	[mm]
	Number	42/47	Inner/outer
	Elastic Modulus	210	[GPa]

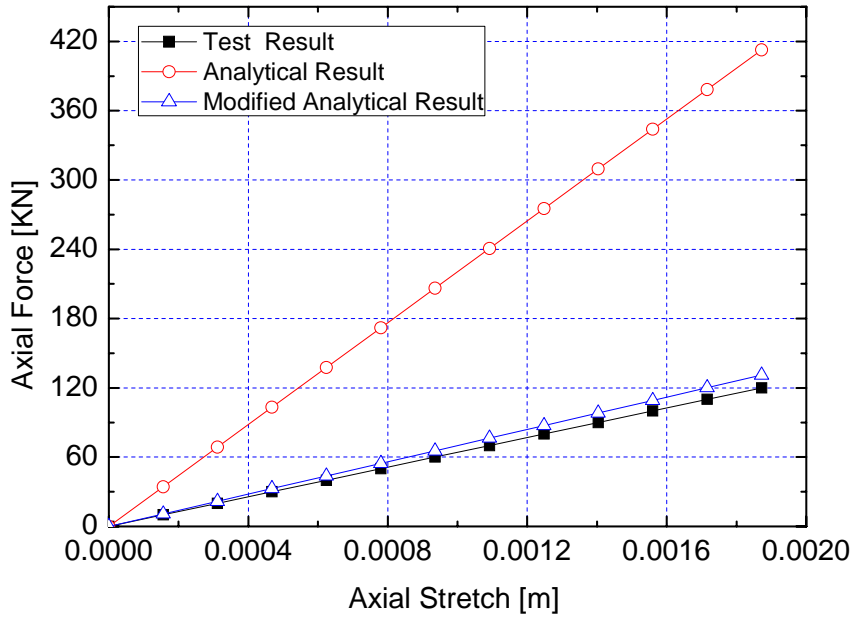


Fig. 6 Measured and calculated axial load versus axial stretch

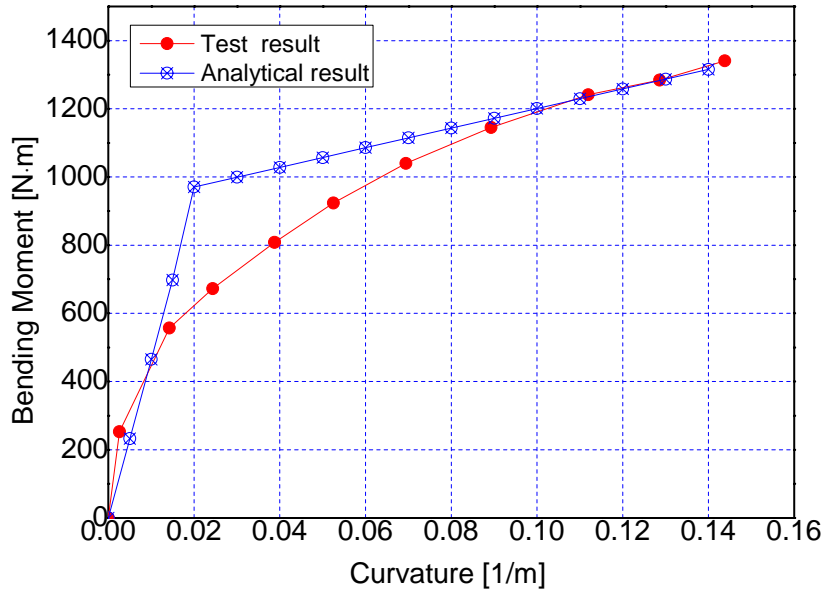


Fig. 7 Measured and calculated bending moment versus bending curvature

Fig. 6 demonstrates that the analytical axial stiffness is $3.79 \times 10^5 \text{ KN}$, which is almost three times as the results measured from the corresponding experiment. The differences between the two results are attributed to the fact that the radius reduction of helical tendon is neglected in the analytical model, which is induced by the contractions of central assembly and insertions of the helical tendon with the sheaths. The similar trends and differences have also been reported by reference (Ekeberg *et al.* (2006)). To consider the effect of the radius reduction of helical tendon, a modify axial stiffness formula has been introduced as

$$K_a = \sum_{i=1}^n A_i E_i \cos \alpha_i (\cos^2 \alpha_i - \nu \sin^2 \alpha_i) + \sum_{j=1}^m A_j E_j \quad (65)$$

where ν is the ratio of radius reduction which denotes the relationship between the radius reduction and the axial elongation of the helical tendon. Considering ν equals to 5 in this example, we can get an excellent axial stiffness predicting result compared with the test result.

Fig. 7 demonstrates the analytical bending stiffness is $4.65 \times 10^4 \text{ N}\cdot\text{m}$ under stick state and $2.87 \times 10^3 \text{ N}\cdot\text{m}$ under slip state, which have satisfactory agreements with the results measured in the corresponding experiment. The difference in the curves of the analytical and measured results is caused by the assumption that all umbilical components are of the same friction coefficient, which in fact varies among the components in the real conditions. The bending stiffness under stick state is much larger than that under slip state, which can prove that the friction has considerable effects on the bending stiffness of the umbilical.

3.3 Extreme strength and fatigue life estimation

Step 1. Sea states description

The umbilical is supposed to be applied in South China Sea area with water depth of 1500m. The joint distribution probabilities of significant wave height and peak period is adopted to define the long-term description of this sea area, as illustrated in Table 3. The table shows, for instance, that the probability of significant wave height between 1.0 and 1.5 and the spectral peak period between 5 and 6 is 12.46%.

As shown in Table 3, the sea states are numerous. To simplify, 12 representative sea states with relatively greater probability are selected to represent practical sea states. The equivalent probabilities of the selected sea states can be calculated by

$$P_{ij} = \sum P_{ik} \quad (66)$$

where P_{ij} denotes the equivalent probability of selected sea states with significant wave height i and peak period j , P_{ik} denotes the probability of adjacent sea states with significant wave height i and close value k of peak period

Table 4 shows the selected sea states according to the real environment of the umbilical working field.

Step 2. Tension force and bending curvature on the critical point

The RAOs of the floating platform system including the platform, morning lines and risers can

be obtained by coupled analysis.

Table 3 Joint distribution probability of each significant wave height and spectral peak period

Significant wave height (m)	Spectral peak period (s)									Probability Sum (%)
	<3	3-4	4-5	5-6	6-7	7-8	8-9	9-10	>10	
0.0≤0.5	0	2.27	11.62	2.37	0.02	0	0	0	0	16.28
0.5≤1.0	0	0.40	19.17	17.02	0.64	0.07	0.01	0	0	37.31
1.0≤1.5	0	0	5.76	12.46	3.15	0.06	0.02	0	0	21.45
1.5≤2.0	0	0	0.25	5.80	4.61	0.22	0	0	0	10.88
2.0≤2.5	0	0	0	1.61	4.19	0.39	0.03	0	0	6.22
2.5≤3.0	0	0	0	0.21	2.73	0.37	0	0	0	3.31
3.0≤3.5	0	0	0	0	1.77	0.51	0	0	0	2.28
3.5≤4.0	0	0	0	0	0.37	0.66	0	0	0	1.03
4.0≤4.5	0	0	0	0	0.09	0.59	0	0	0	0.68
4.5≤5.0	0	0	0	0	0.01	0.28	0	0	0	0.29
5.0≤6.0	0	0	0	0	0	0.17	0.03	0	0	0.2
6.0≤7.0	0	0	0	0	0	0.04	0.03	0	0	0.07
>7.0	0	0	0	0	0	0	0	0	0	0
Probability Sum (%)							100.00			

Table 4 Selected sea states parameters

Sea number	Significant wave height (m)	Spectral peak period (s)	Probability (%)
1	0.5	4	16.28
2	1	4	19.57
3	1	6	17.74
4	1.5	6	18.22
5	1.5	7	3.23
6	2	6	6.05
7	2	7	4.83
8	2.5	6	6.22
9	3	6	3.31
10	4	7	3.31
11	5	7	0.97
12	7	8	0.27
Sum of probability (%)		100	

Then global dynamic tension and curvature of the umbilical under each sea state can be calculated by coupled time domain analysis based on the FEM (Orcaflex Manual). Figs. 8 and 9 show the maximum and minimal tension force and bending curvature distributions under sea state No.12 as an example.

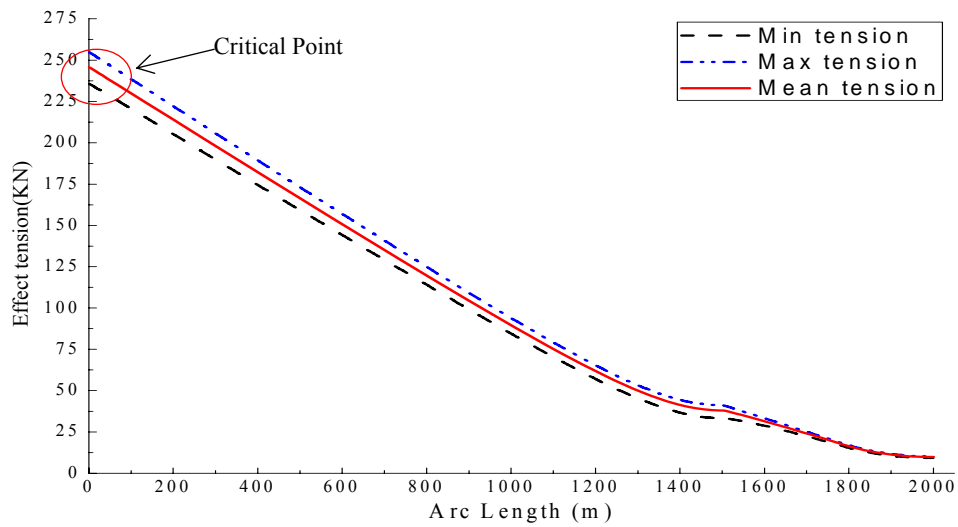


Fig. 8 Tension distribution along the umbilical under sea state No.12

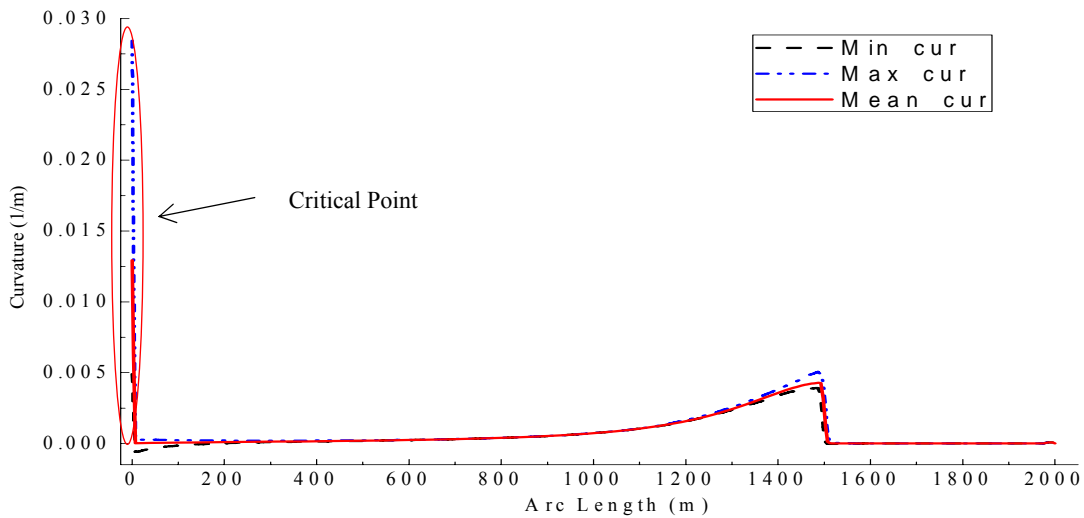


Fig. 9 Curvature distribution along the umbilical length under sea state No.12

Figs. 8 and 9 demonstrate that the maximal changing magnitude of the tension force and curvature occurred at the top hanging off point due to the fact that the top point of the umbilical has the largest tension and motions angles in every sea state. Therefore, the top point of the umbilical is chosen as the critical point for extreme and fatigue life evaluation. The corresponding time series of the tension and curvature of this critical point within 0.5 hour is further illustrated in Figs.10 and11.

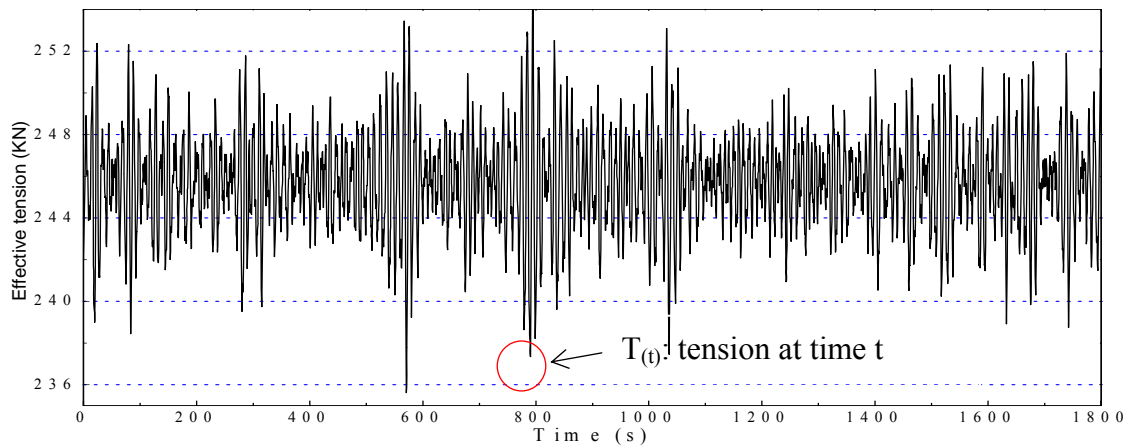


Fig. 10 Effective tension time series of the critical point within 0.5 hour under sea state No.12

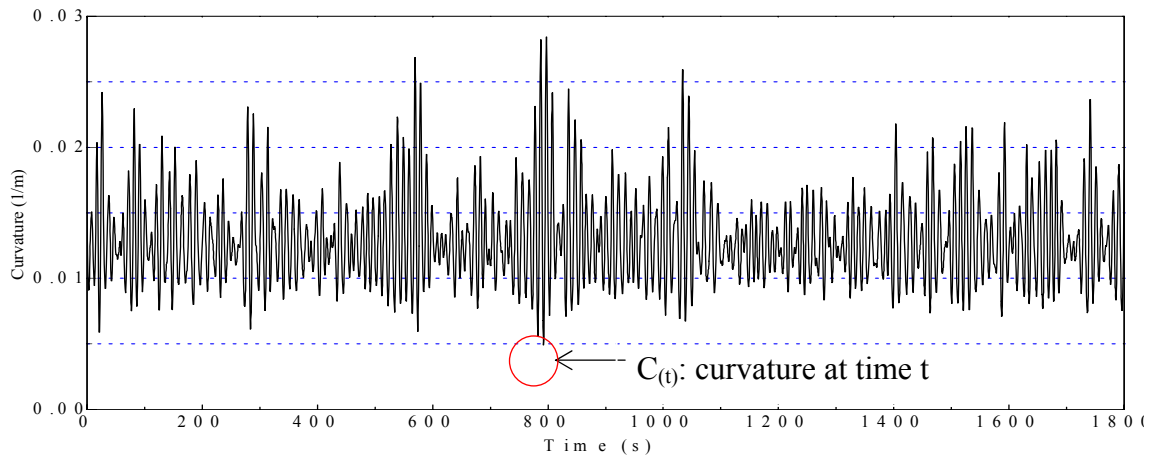


Fig. 11 Curvature time series of the critical point within 0.5 hour under sea state No.12

As shown in Figs. 10 and 11, the tension force and curvature fluctuate around 246 kN and 0.0125rad/m respectively, and simultaneously reach their maximum values at around 800s, which indicates that the umbilical reaches the maximum stress conditions at this moment. Hence the extreme strength evaluation would be performed at this condition.

Step 3. Extreme strength evaluation

Given design geometrical parameters and material properties, the extreme capacity of the umbilical under tension and bending loads can be obtained using Eq. (64) and represented by the area enclosed by the horizontal axis (Curvature), vertical axis (Tension Force) and the calculated extreme capacity lines at the tension-curvature condition. Fig. 12 shows the extreme strength evaluation results for the umbilical, where 100% and 80% utilization of the ultimate strength of the material are considered. The figure also indicates that, to make the umbilical meet the extreme strength requirement, given a certain curvature value there should be a limited tension force, and vice versa.

Therefore, it is clear that to avoid the failure of the umbilical, the tension-curvature trajectories obtained via the global analysis should be within the extreme strength limitation area. For the numerical case in this paper, the tension-curvature trajectories are plotted in Fig. 12 using the blue lines. Obviously, the tension force and curvature trajectories of the critical point are within the extreme strength limitation skylines. Therefore, we can claim that this umbilical design meets the extreme strength requirements.

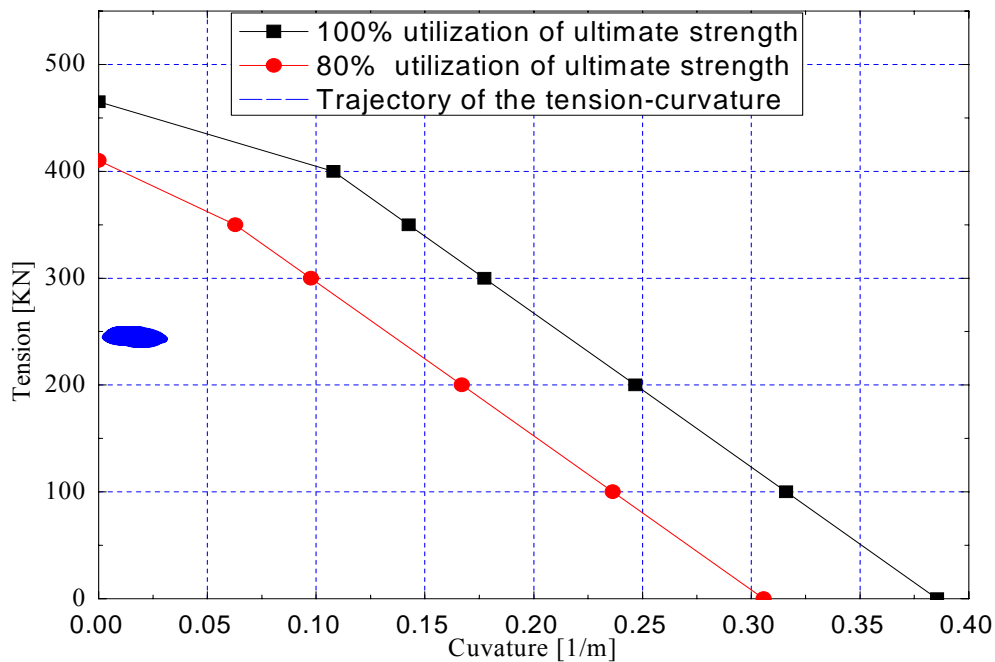


Fig. 12 Extreme strength skylines and calculated tension-curvature trajectory

Step 4. Fatigue stress calculation

As illustrated in Fig. 9, the mean tension force is 246 kN and then the contact pressure of tube component can be calculated by Eq. (44)

$$q^i = q^e = \frac{FEA \cos^3 \alpha \sin \alpha}{RK_a} + \frac{2\pi RP}{k} = 5660 \text{ (kN/m)} \quad (67)$$

Substituting the result of contact pressure into Eq. (45), we obtain the critical bending curvature

$$1/R_{yc} = \frac{\mu(q^i + q^{i+1})}{EA \cos^2 \alpha \sin \alpha} = 0.0367 \text{ (1/m)} \quad (68)$$

where the friction coefficient μ is defined to be 0.15 according to the material test.

Evidently, all curvatures in Fig. 10 are under the critical bending curvature, and we can draw a conclusion that the tube component is under stick state. Then based on the time series of the tension forces and the bending curvatures obtained above, the stress inside the umbilical's tube component at the critical point can be calculated by Eq. (55). The corresponding results of the numerical example are plotted in Fig. 13.

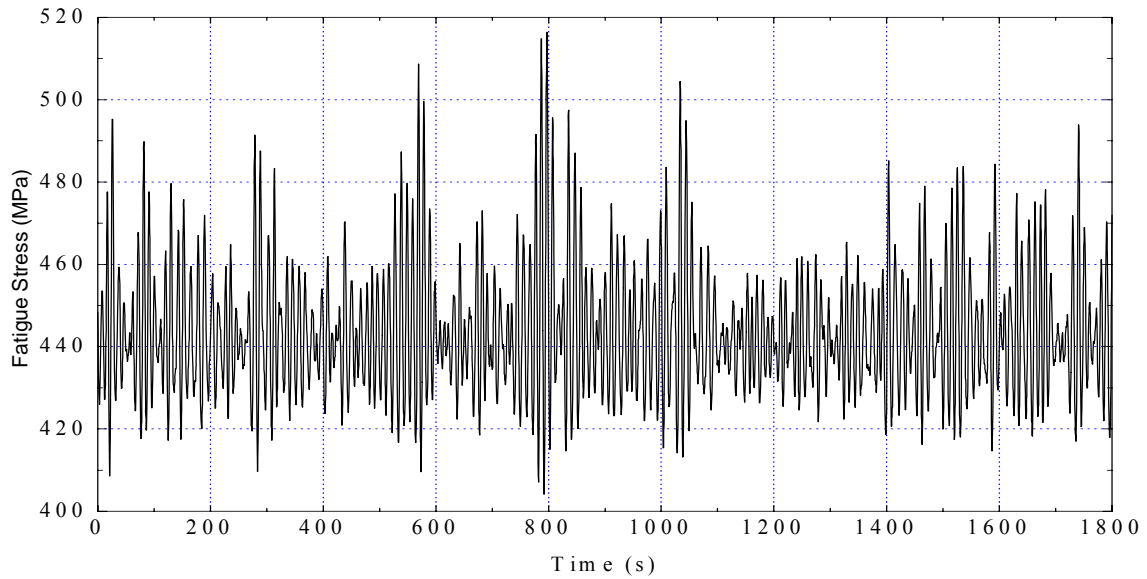


Fig. 13 Fatigue stress time series of the critical point under sea state No.12

Fig. 13 shows the fatigue stress time series of tube component at critical point under the tension forces and bending curvatures. Comparing the values in Figs. 10, 11 and 13, we can see that the significant values appeared simultaneously, which can attribute to the fact that the fatigue stresses resulted from tension and curvature are of linear superposition. Fig. 13 also demonstrates that the variations of fatigue stresses are random and indescribable; therefore, it is necessary to use the cycle counting algorithm named Rainflow counting to calculate the ranges and cycles of fatigue stresses.

Step 5. Determination of stress ranges and cycle

Using Rainflow counting (Socie (1991)), we can obtain the changing ranges and mean values in the fatigue stress time history at the critical point under each sea state and the corresponding cycles appearing in one year. To consider the mean stress level effects on the fatigue damages, the obtained stress ranges should be further corrected by Goodman line (Knapp (2004))

$$\frac{\sigma_a'}{\sigma_f} + \frac{\sigma_m'}{\sigma_{ut}} = 1 \quad (69)$$

where, σ_f , σ_a' , σ_{ut} and σ_m' are the equivalent fatigue stress range, the calculated fatigue stress range, the ultimate stress and the mean stress, respectively.

Considering the happening probabilities of each sea state, we can finally obtain the total cycles n of each equivalent fatigue stress ranges appearing in one year by

$$n = \sum_{i=1}^{12} n_i P_i \quad (70)$$

where n_i denotes cycles of a certain equivalent fatigue stress ranges appearing in one year under sea state i ; P_i denotes happening probabilities of sea state i . And the corresponding results for the considered umbilical are shown in Fig. 14.

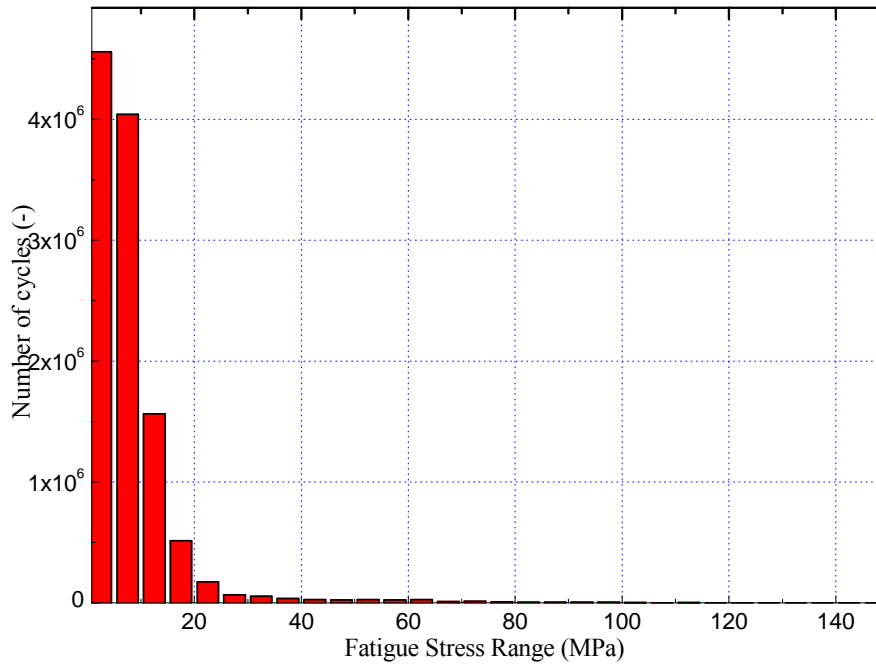


Fig. 14 Cycle numbers of each stress range in one year under all sea states

Fig. 14 shows the distribution of cycle numbers as a function of stress range, where the cycles will decrease with the increase of the equivalent fatigue stress range. The results can be explained by the fact that the reiterations of small variation ranges of fatigue stress are much more than those of large ones, as shown in Fig. 13.

Step 6. Fatigue life estimation

The S-N curve is adopted in fatigue life prediction of the umbilical; and for the case in this paper, the following S-N curve is used (DNV-RP-C203 (2010))

$$\log(N) = 13.785 - 3.5 \log(\Delta\sigma)$$

where N is the number of cycles when the material is failed under stress range $\Delta\sigma$.

With the chosen S-N curve, the fatigue damage in one year of fatigue stress range i can be calculated by

$$\nu_i = \frac{n_i}{N_i} \quad (71)$$

where ν_i denotes fatigue damage of fatigue stress range σ_i , n_i denotes the cycles of fatigue stress range σ_i in one year and N_i denotes the cycles-to-failure of fatigue stress range σ_i . The corresponding results for the case in this paper are shown in Fig. 15.

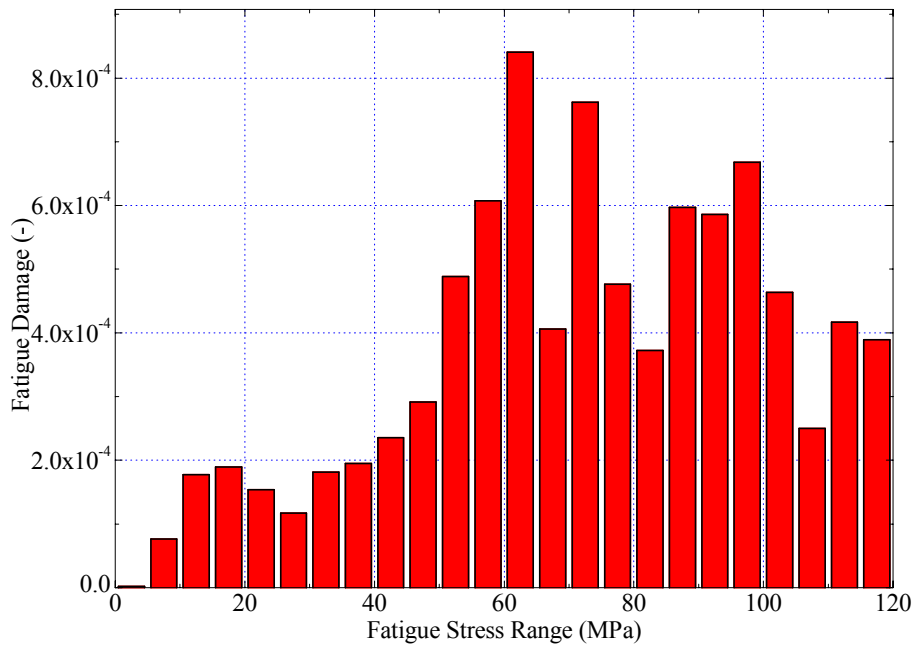


Fig. 15 Fatigue damage of each stress range in one year

Fig. 15 indicates that the largest fatigue damage is from the stress rang 60-65 MPa, whereas the 0-5MPa stress range is the smallest part. Stress range between 50 to 120 MPa will serve as the primary contribution to the fatigue damage. Summing all of the fatigue damages induced by each stress range, the fatigue damage ν in one year can then be obtained as

$$\nu = \sum v_i = 0.0096 \quad (72)$$

Therefore, the fatigue life of this umbilical can be estimated by

$$n = \frac{1}{\nu} = \frac{1}{0.0096} = 104 \quad (73)$$

The fatigue life of the umbilical determined by the tube components is 104 years

4. Conclusions

The analytical model of the un-bonded umbilical for sectional stress calculation has been presented in this paper. The stress in this analytical model is constituted by tensional stress and bending stress. Based on the Hook's law, tensile stress is obtained by deducing the axial strain of helical components. Considering the effects of the friction of helical components, the bending stress is divided into elastic bending stress and friction stress. The elastic bending stress is obtained by deducing the curvature of helical components and the friction stress is calculated by determining the shear stress before and after the helical components' slipping. Based on the analysis, comparatively straightforward analytical models for stress and stiffness are proposed to apply in the umbilical design.

Analytical axial and bending stiffness have been compared with experimental data and encouraging agreements have been found. The comparisons prove that the radius reduction and friction has a great effect on the axial and bending stiffness respectively.

Combined with standard dynamic numerical simulation methods for the risers, the model can be used to estimate the extreme capacity and fatigue life of un-bonded umbilical. As testified by the numerical example, the analytical model is applicable in the design of un-bonded umbilicals.

Acknowledgments

This work was financially supported by the National Natural Science Foundation of China (Grant No. 51009088 and No. 51279101).

References

- Costello, G.A. (1997), *Theory of Wire Rope* (2th Ed), Springer, New York, USA.
- DNV-OS-F101(2005), Submarine Pipe Systems.
- DNV-RP-C203 (2010), Fatigue Design of Offshore Steel Structures.
- Ekeberg, K.I., Ottesen, T., Aarstein, J., Nexans Norway A/S, Saevik, S., Ye, N. and Marintek, R.I. (2006),

- “Measuring and implementing friction and bending stresses in dynamic umbilical design”, *Proceedings of the Offshore Technology Conference*, Houston, May.
- Ferét, J. and Bournazel, C.L. (1987), “Calculation of stress and slip in structural layers of un-bonded flexible pipes”, *J. Offshore Mech. Arct.*, **109** (1), 263-269.
- ISO 13628-5 (2005), Design and Operation of Subsea Production Systems-Subsea Umbilicals.
- Knapp, R.H. (1979), “Derivation of a new stiffness matrix for helically armored cables considering tension and torsion”, *Int. J. Numer. Meth. Eng.*, **14** (4), 515-529.
- Knapp, R.H. (2004), “Tension and bending fatigue modeling of cables”, *Proceedings of the 14th International Offshore and Polar Engineering Conference*, Toulon, France, May.
- Lipschutz, M.M. (1969), *Differential Geometry*, McGraw-Hill, New York.
- Martins, C.A. and Pesce, C.P. (2002), “A simplified procedure to assess the fatigue-life of flexible risers”, *Proceedings of the 12th International Offshore and Polar Engineering Conference*, Kitakushu, Japan, May.
- OrcaFlex Manual (2006), Version 9.0a, Orcina Ltd, U.K.
- Seavik, S. (2011), “Theoretical and experimental studies of stresses in flexible pipes”, *Appl. Ocean Res.*, **27**(2), 97-106.
- Socie, D. (1991), *Rainflow cycle counting: a historical perspective*, Butterworth-Heinemann, Oxford, U.K.
- Thies, P.R., Johannig, L. and Smith, G.H. (2011), “Assessing mechanical loading regimes and fatigue life of marine power cables in marine energy applications”, *Proceedings of the IMechE, Part O: J Risk and Reliability*, **226**(1), 18-32.
- Witz, J. and Tan, Z. (1995), “Rotary bending of marine cables and umbilicals”, *Eng. Struct.*, **17**(4), 267-275.
- Witz, J.A. and Tan, Z. (1996), “On the axial-torsional structural behaviour of flexible pipes, umbilicals and cables”, *Mar. Struct.*, **9**(2-3), 205-227.
- Witz, J.A. and Tan, Z. (1996), “On the flexural structural behaviour of flexible pipes, umbilicals and marine cables”, *Mar. Struct.*, **9**(2-3), 229-249.